Progress in Neurobiology 220 (2023) 102374

Contents lists available at ScienceDirect

Progress in Neurobiology

journal homepage: www.elsevier.com/locate/pneurobio

Two fine-scale channels for encoding motion and stereopsis within the human magnocellular stream

B. Kennedy [a], P. Bex [b], D.G. Hunter [c,d], S. Nasr [a,e,*]

[a] Athinoula A. Martinos Center for Biomedical Imaging, Massachusetts General Hospital, Charlestown, MA, United States
[b] Department of Psychology, Northeastern University, Boston, MA, United States
[c] Department of Ophthalmology, Harvard Medical School, Boston, MA, United States
[d] Department of Ophthalmology, Boston's Children Hospital, Boston, MA, United States
[e] Department of Radiology, Harvard Medical School, Boston, MA, United States

ARTICLE INFO

Keywords:
Extrastriate cortex
Visual processing
Mesoscale functional organization
High resolution fMRI
Ultra-high field (7T) scanner

ABSTRACT

In humans and non-human primates (NHPs), motion and stereopsis are processed within fine-scale cortical sites, including V2 thick stripes and their extensions into areas V3 and V3A that are believed to be under the influence of magnocellular stream. However, in both species, the relative functional organization (overlapping vs. none overlapping) of these sites remains unclear. Using high-resolution functional MRI (fMRI), we found evidence for two minimally-overlapping channels within human extrastriate areas that contribute to processing motion and stereopsis. Across multiple experiments that included different stimuli (random dots, gratings, and natural scenes), the functional selectivity of these channels for motion vs. stereopsis remained consistent. Furthermore, an analysis of resting-state functional connectivity revealed stronger functional connectivity within the two channels rather than between them. This finding provides a new perspective toward the mesoscale organization of the magnocellular stream within the human extrastriate visual cortex, beyond our previous understanding based on animal models.

1. Introduction

In the visual cortex of humans and NHPs, the magnocellular processing stream consists of multiple fine-scale cortical sites that are distributed across extrastriate visual cortex (Felleman and Van Essen, 1991; Tootell and Nasr, 2017). In both species, these cortical sites are involved in processing motion and stereopsis (depth), two important but fundamentally different aspects of any visual stimuli. To this day, in either species, it remains unknown whether motion and stereopsis are encoded within two mostly separate (i.e. none-to-minimally overlapping) sites within the magnocellular stream or if the same sites contribute to encoding both features.

In NHPs, stimulus motion and stereopsis are processed selectively within V2 thick stripes (Chen et al., 2008; Hubel and Livingstone, 1987; Li et al., 2017; Lu et al., 2010; Maunsell and Van Essen, 1983; Peterhans and von der Heydt, 1993; Roe and Ts'o, 1995; Shipp and Zeki, 2002). The information encoded within these stripes is further processed within areas V3, V3A and MT (Felleman and Van Essen, 1991; Zeki and Shipp, 1988). Specifically, motion-selective neuronal columns are found frequently within areas V3 (Felleman and Van Essen, 1987; Gegenfurtner et al., 1997), V3A (Galletti et al., 1990; Nakhla et al., 2021; Zeki, 1978) (but see also (Orban et al., 2003; Vanduffel et al., 2001)) and MT (Albright et al., 1984; DeAngelis and Uka, 2003; Maunsell et al., 1990). Stereo-selective neuronal columns have also been reported within all these areas (Anzai et al., 2011; DeAngelis and Newsome, 1999, 2004; Felleman and Van Essen, 1987; Krug and Parker, 2011; Thomas et al., 2002; Tsao et al., 2003). However, the relative spatial organization of motion- and stereo-selective sites within these areas remains largely unknown.

With recent advances in high-resolution fMRI, homologous organizations have been shown in human visual cortex. Specifically, multiple studies have shown evidence for cortical columns across areas V2, V3 and V3A that contribute to encoding stereopsis (Goncalves et al., 2015; Nasr et al., 2016; Ng et al., 2021) and motion (Tootell and Nasr, 2021). Similar to NHPs, and based on their stimulus selectivity and functional connections, these cortical columns appear to be under the influence of magnocellular stream (Tootell and Nasr, 2017, 2021). Here again, the relative spatial organization of motion- and stereo-selective sites within

* Correspondence to: Bldg. 149, 13th street, Charlestown, MA 02129, United States.
E-mail address: shahin.nasr@mgh.harvard.edu (S. Nasr).

https://doi.org/10.1016/j.pneurobio.2022.102374
Received 20 April 2022; Received in revised form 16 October 2022; Accepted 15 November 2022
Available online 17 November 2022

these early visual areas remains largely unknown due to technical challenges in functional imaging of such small brain sites.

Thus, despite the abundance of evidence for existence of motion- and stereo-selective cortical columns across areas V2, V3 and V3A in humans and NHPs, the detailed nature of their spatial organization (overlapping vs. none (or minimally) overlapping) remains unknown. Consequently, it is not clear whether motion processing is conducted in parallel with that of stereopsis or if the processing of motion is intermixed with that for stereopsis. This lack of knowledge has limited our ability to infer the underlying circuitry at mesoscale levels.

Here, we tested the hypothesis that motion and stereopsis are processed through two minimally-overlapping channels within the human extrastriate visual areas. Using high-resolution fMRI, we localized the fine-scale motion- and stereo-selective sites across areas V2, V3 and V3A in the same individuals. Using this technique, we also tested the functional properties of these sites, including their contribution in orientation, spatial frequency (SF), motion direction and depth encoding plus their functional connections during resting-state. The result of these tests revealed that motion- and stereo-selective sites are distributed within several cortical areas, including V2, V3 and V3A, forming two channels within the magnocellularly influenced regions.

2. Methods

2.1. Participants

Fifteen human subjects (6 females), aged 23–44 years old, participated in this study (Table S1). All subjects had normal or corrected-to-normal visual acuity (based on the Snellen test), normal color vision (Ishihara and Farnsworth D15 tests), normal stereovision (Randot test), and radiologically normal brains without history of neuropsychological disorder. All experimental procedures conformed to NIH guidelines and were approved by Massachusetts General Hospital protocols. Written informed consent was obtained from all subjects prior to all experiments.

2.2. General Procedures

Subjects were scanned multiple times (Table S1) in an ultra-high field 7T scanner (whole-body system, Siemens Healthcare, Erlangen, Germany) for functional experiments. All subjects were also scanned in a 3T scanner (Tim Trio, Siemens Healthcare) for structural imaging.

In all functional experiments (except for the functional connectivity test), stimuli were presented via an LCD projector (1024 × 768 pixel resolution, 60 Hz refresh rate) onto a rear-projection screen, viewed through a mirror mounted on the receive coil array. Matlab 2020a (MathWorks, Natick, MA, USA) and the Psychophysics Toolbox (Brainard, 1997; Pelli, 1997) were used to control stimulus presentation.

All experiments (except for the resting-state tests) were block-designed. The duration of blocks (Table S1), the number of blocks per stimulus condition, and the average luminance of the stimuli did not differ between the experimental conditions. Further details of the stimuli are described separately for each experiment below.

During these experiments, subjects were instructed to look at a centrally presented object (radius = 0.15°) and to do an orthogonal dummy task. Specifically, in all experiments (except for resting state and the stereo-selectivity tests), subjects were asked to report color-change for the fixation target (red-to-blue or vice versa). For the stereo-selectivity tests, subjects were asked to report shape-change for the fixation target (circle-to-square or vice versa). These tasks were conducted irrespective of the stimuli presented in the background and remained the same across the whole run, including the blank presentation interval. In all experiments, the subject's average performance for the dummy task remained above 75 % without any significant difference across experimental conditions ($p > 0.10$).

2.2.1. Experiment 1a – Localizing motion-selective sites

Motion-selective sites were localized based on their stronger response to moving compared to stationary stimuli. Stimuli consisted of concentric rings (30 cd/m^2), extending 20° × 26° (height × width) in the visual field, presented against a light gray background (40 cd/m^2) (Fig. 1A). As mentioned above, the experiment was block-designed (24 s per block; Table S1). In half of the blocks, rings moved radially (centrifugally vs. centripetally; 4°/s) and the direction of motion changed every 3 s to reduce the impact of motion after-effects. In the other half of blocks, rings remained stationary during the whole block. Each run started and finished with a 12 s of uniform gray presentation. The sequence of moving and stationary blocks was pseudo-randomized across runs.

2.2.2. Experiment 1b – Localizing stereo-selective sites

Stereo-selective sites were localized based on their stronger response to 3D compared to 2D stimuli. Stimuli were sparse (5 %) random dot stereograms (RDS), based on red or green dots (0.09° × 0.09°; 56 cd/m^2), presented against a black background (Fig. 1B). Stimuli extended 20° × 26° in the visual field. Subjects viewed the stimulus through custom made anaglyph spectacles mounted to the head coil. In the 3D blocks (24 s per block; Table S1), the RDS stimuli formed a stereoscopic percept of an array of cuboids that oscillated in depth (−0.22° to 0.22°; 0.3 Hz), with independent phase. In the 2D blocks, the fused percept formed a fronto-parallel plane intersecting the fixation target (i.e. zero depth at that point) and oscillated translationally (left to right and vice versa; 0.3 Hz). Each experimental run began and ended with 12 s of uniform black. The sequence of stimulus blocks was pseudo-randomized across runs.

2.2.3. Experiments 2a and 2b – Localizing color-selective sites and measuring the impact of stimulus orientation on the evoked response

To localize color-selective sites, subjects were presented in separate blocks (24 s per block; Table S1) with sinusoidal gratings (0.2c/deg; 20° × 26°) which varied in either color (between red and blue) or achromatic luminance (Fig. 1C). For each subject, colors were adjusted to be equal in luminance across all eccentricities stimulated, using the method of flicker-photometry (Bone and Landrum, 2004; Ives, 1907) and according to each subject's color perception (for more details see (Nasr et al., 2016)).

In different blocks, orientation of colorful and achromatic gratings were either 0°, 45°, 90° or 135°, drifting in orthogonal directions (reversed every 6 s) at 4°/s. This design enabled us to measure the impact of stimulus orientation on the evoked response (Experiment 2b). Each run started and finished with a short block (18 s) of uniform gray of equal mean luminance. The sequence of blocks within each run was pseudo-randomized.

2.2.4. Experiment 2c – Measuring spatial frequency preference

To measure the spatial frequency preference in different sites, subjects were presented with sinusoidal gratings (20° × 26°; average luminance = 40 cd/m^2) of differing spatial frequency (0.1, 0.27, 0.73, 2.08 and 5.79c/deg) across different blocks (16 s per block; Table S1). In each block, the spatial frequency of the stimuli remained the same. But the orientation of gratings changed pseudo-randomly every 4 s. In addition, grating phase reversed every 1 s. Each run began and ended with an additional block (12 s) of uniform gray of equivalent mean luminance. The sequence of blocks was pseudo-randomized across runs.

2.2.5. Experiment 3a – Measuring motion-selective activity induced by radially-moving random dots

In this experiment, rather than using concentric rings (as in Experiment 1a), subjects were presented with white (80 cd/m^2) random dots (Fig. 4A). In different blocks (24 s per block; Table S1), dots moved (4°/s) either centrifugally (33 % of blocks), centripetally (33 % of blocks) or remained stationary (the rest of blocks). This design also enabled us to

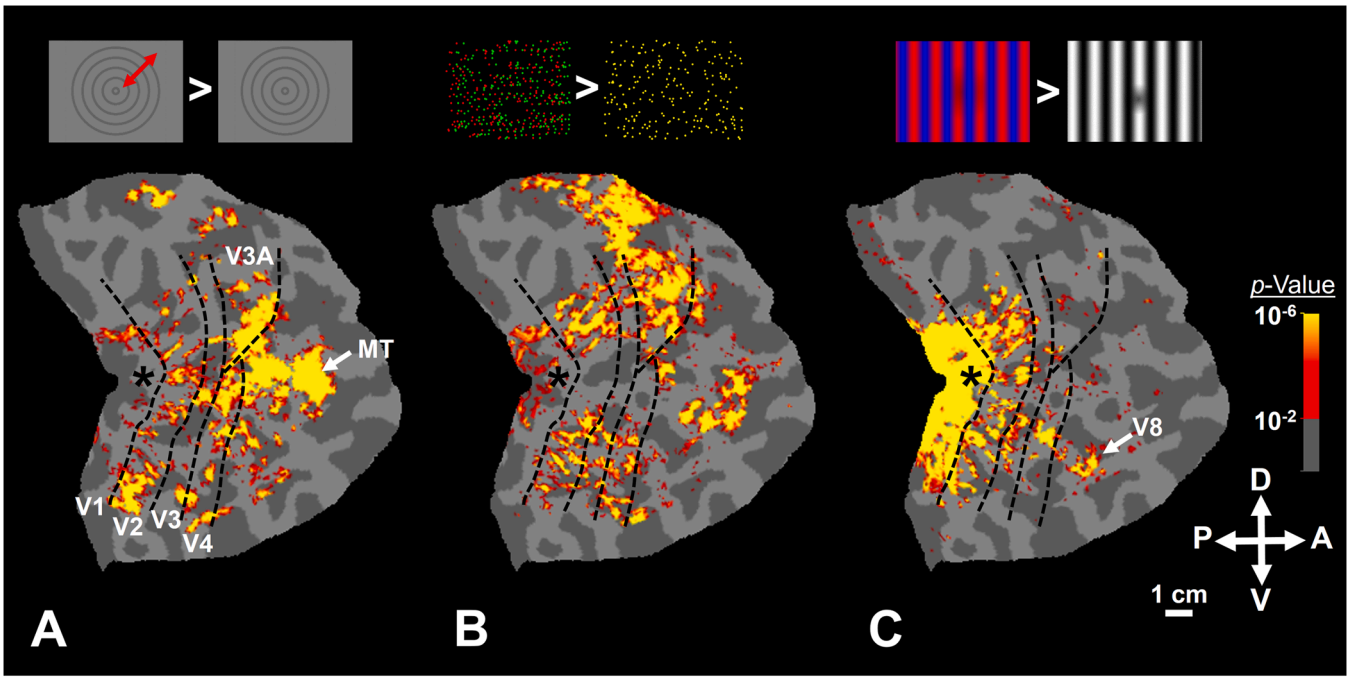

Fig. 1. Motion, stereopsis and color evoke selective activity within the extrastriate cortex of one individual subject (right hemisphere), overlaid on the subject's flattened cortex (Experiments 1 and 2a). Panels show the selective activity evoked by contrasting the response to moving vs. stationary (**Panel A**), 3D vs. 2D RDS (**Panel B**) and color- vs. luminance-varying stimuli (**Panel C**). A schematic representation of the stimuli is also illustrated on top of each panel (see Methods). In all experiments, we detected stripy activity sites, starting at V1-V2 border that extended into areas V3 and V4. The stripy/patchy pattern of activity in areas V2 and V3 is consistent with the expected shape of stripes reported in histological studies (Tootell and Taylor, 1995; Adams et al., 2007). As reported previously (Tootell and Nasr, 2017), color-selective sites were rarely detected within area V3A. In each panel, the border of retinotopic visual areas is shown with black dashed lines (see Methods and Fig. S1). The asterisks show the foveal representation in area V1. The location area MT (**Panel A**) and V8/VO (**Panel C**) are indicated by white arrows.

assess the impact of motion direction (centrifugal vs. centripetal) on the evoked response (Experiment 5a). Stimuli were presented against a black background, extending 20° × 26° in the visual field. The size of dots increased with eccentricity according to cortical magnification factor (Sereno et al., 1995). Each run began and ended with an additional block (12 s) of uniform black. The sequence of blocks was pseudo-randomized across runs.

2.2.6. *Experiment 3b – Measuring motion-selective activity induced by translationally- moving random dots*

The stimuli were similar to those used in Experiment 3a with two exceptions. First, rather than moving radially, in different blocks (24 s per block; Table S1), stimuli moved either left-ward (20 % of blocks), right-ward (20 % of block), up-ward (20 % of block), and down-ward (20 % of block) (Figure S7). In the rest of blocks, stimuli remained stationary. Second, the size of dots remained the same (radius = 0.02°) and did not change with their eccentricity. This design also enabled us to measure the impact of motion direction on the evoked response (Experiment 5b). The other aspects of the procedure were similar to those in Experiment 3a.

2.2.7. *Experiment 3c – Measuring stereo-selective activity induced by depth-varying gratings*

In this experiment, rather than using RDS to measure stereo-selective activation, (as in Experiment 1b), subjects were presented with low SF (0.25c/deg) red-to-black and green-to-black sinusoidal gratings (20° × 26°; average luminance = 28 cd/m^2) (Fig. 4C). Subjects viewed the stimuli through custom anaglyph spectacles as in Experiment 1b. Stimuli overlaid and fused within all experiment blocks. In 50 % of blocks (24 s per block; Table S1), the level of binocular disparity oscillated between − 0.22 and 0.22° (0.3 Hz), forming a stereoscopic percept of oscillation in depth. In the rest of blocks, the level of binocular disparity remained equal to zero and stimuli formed a perception of oscillation in the fronto-parallel plane. The orientation of gratings varied pseudo-randomly between blocks. The other aspects of the procedure was similar to Experiment 1b.

2.2.8. *Experiment 4 – Measuring stereo-selective activity induced by 3D natural scenes*

Subjects were presented with 3D vs. 2D scenes (Figure S8A) across different blocks. Stimuli included pictures of indoor and outdoor scenes, selected from Southampton-York Natural Scenes (SYNS) dataset (Adams et al., 2016). Each stimulus extending 20° × 26° of visual field (average luminance = 36 cd/m^2). Subjects viewed the stimuli through custom anaglyph spectacles as in Experiments 1b. For 3D stimuli, the level of binocular disparity varied between − 0.15 and 0.15° in different parts of each image. Each block contained 24 stimuli (1 s per stimuli) with no blank presentation between the stimuli (Table S1). Each run began and ended with an additional block (12 s) of uniform black presentation. The sequence of stimuli within the blocks and the sequence of blocks within the runs were pseudo-randomized.

2.2.9. *Experiment 5 – Measuring the impact of motion direction and depth on the evoked response*

The impact of motion direction (Experiments 5a and 5b) was measured based on the data collected during Experiments 3a and 3b (see above). To measure the impact of stimulus depth (in front vs. behind fixation plane) on the response evoked within stereo- and motion-selective sites (Experiment 5c), subjects were presented with RDS stimuli (20° × 26°) similar to those used in Experiment 1b. But here, in different blocks (24 s per block; Table S1), stimuli were oscillating (0°−0.22°) either 'in front' or 'behind' a fronto-parallel plane that intersected the fixation target. Other details of the stimuli are similar to those in Experiment 1b.

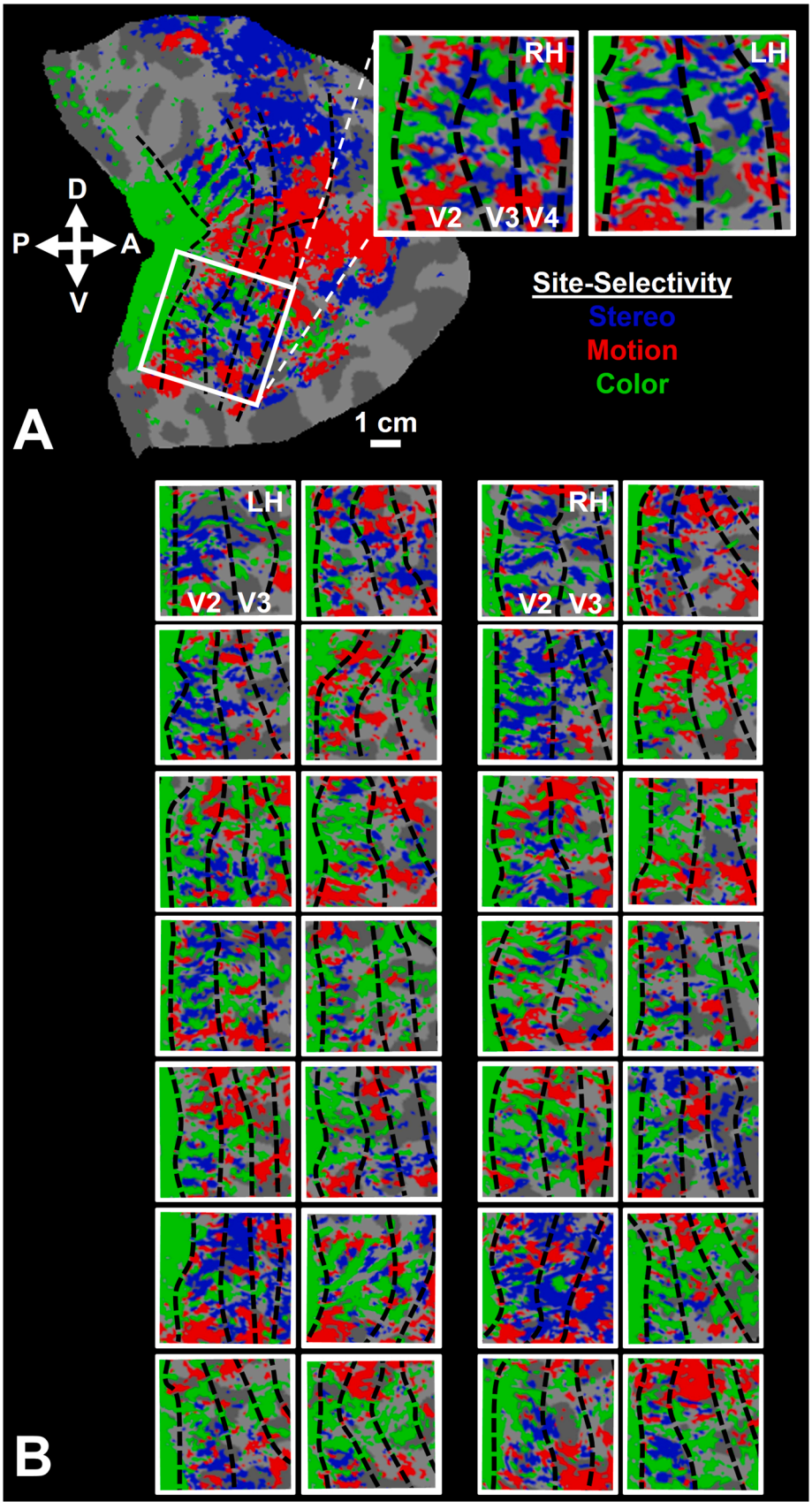

Fig. 2. The co-localization of motion-, stereo- and color-selective sites (Experiments 1 and 2a). **Panel A** shows the data from the same individual as in Fig. 1. **Panel B** shows the spatial distribution of motion-, stereo-, and color-selective sites in twenty-eight hemispheres other than the ones showed in **Panel A**. The left and right columns show data from left and right hemispheres, respectively. In all hemispheres, the selective sites are distributed in areas V2 and V3. Although these examples represented an approximately similar location in all individuals, the heterogeneity and the between-subjects-variability in the spatial organization of these sites have remained apparent. Notably, the overlapping regions are excluded from the maps (but see Figs. S3 and S4 and also Tables S2 and S3). The border of the retinotopic visual areas (black dashed lines) were defined functionally for each subject (see Methods and Figure S1).

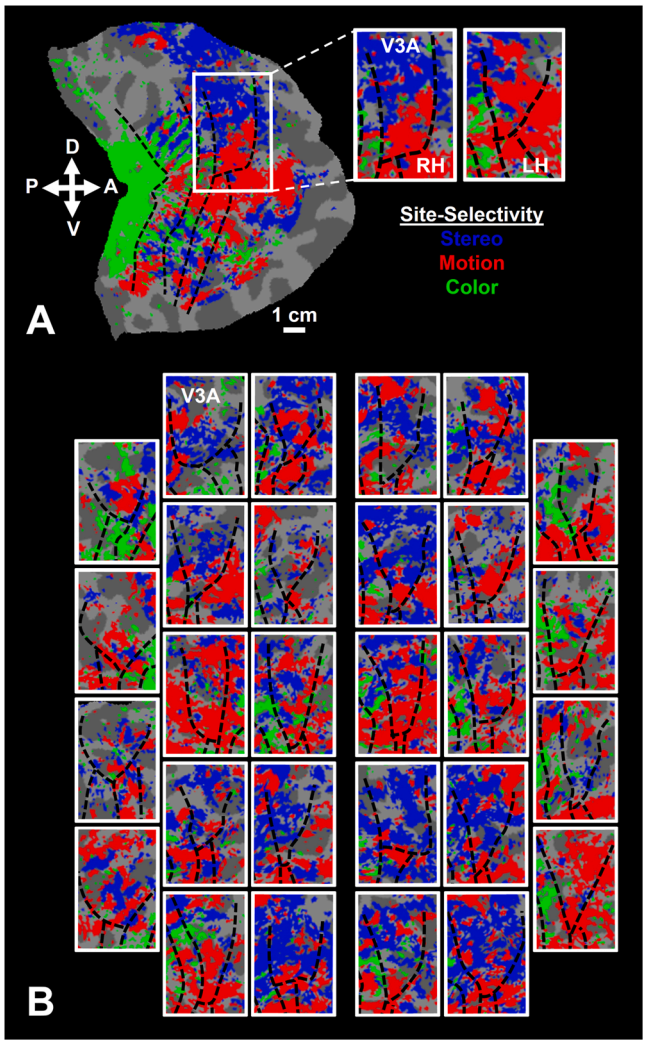

Fig. 3. The co-localization of motion-, stereo- and color-selective sites in area V3A (Experiments 1 and 2a). **Panel A** shows area V3A from the same individual as in Figs. 1 and 2A. **Panel B** shows the same data from twenty-eight other hemispheres. The overall organization of **Panel B** is similar to Fig. 2B. In all hemispheres, motion- and stereo-selective sites are apparent in V3A, while color-selective sites are rarely detected in this area. This effect is similarly observed in left and right hemispheres. Here again, the overlapping regions are not shown (but see Figure S4 and Table S4). As in Fig. 2, the heterogeneity and the between-subjects-variability in extent and in the exact location of these sites is apparent. Other details are the same as Fig. 2.

2.2.10. *Experiments 6 and 7 – Measuring resting-state functional connectivity and time-course signal-to-noise ratio*

During resting-state scans (Experiment 6), subjects were instructed to keep their eyes closed during the whole scan, but not to sleep. Each scan session consisted of 6 runs (Table S1), and each run took 256 s. Experimenters talked to the subject between runs to ensure wakefulness. The same data were also used in Experiment 7 to examine the time-course signal-to-noise ratio of the fMRI signal collected within motion- and stereo-selective sites.

2.2.11. *Retinotopic Mapping*

For all subjects the border of retinotopic areas and the representation of central (radius = 0–3°) and peripheral (radius = 3–10°) visual fields were defined retinotopically (Sereno et al., 1995) (Figure S1). Stimuli were based on a flashing radial checkerboard, presented within retinotopically limited apertures, against a gray background. These retinotopic apertures included wedge-shaped apertures radially centered along the horizontal and vertical meridians (polar angle = 30°), plus a central disk (radius = 0–3°) and a peripheral ring (radius = 3–10°). These stimuli were presented to subjects in different blocks (24 s per block). The sequence of blocks was pseudo-randomized across runs (8 blocks per run) and each subject participate in at least 4 runs.

2.3. *Imaging*

Functional experiments (see above) were conducted in a 7T Siemens whole-body scanner (Siemens Healthcare, Erlangen, Germany) equipped with SC72 body gradients (70 mT/m maximum gradient strength and 200 T/m/s maximum slew rate) using a custom-built 32-channel helmet receive coil array and a birdcage volume transmit coil. Voxel dimensions were nominally 1.0 mm. We used single-shot gradient-echo EPI to acquire functional images with the following protocol parameter values: TR = 3000 ms, TE = 28 ms, flip angle = 78°, matrix= 192 × 192, BW= 1184 Hz/pix, echo-spacing = 1 ms, 7/8 phase partial Fourier, FOV = 192 × 192 mm, 44 oblique-coronal slices, acceleration factor $R = 4$ with GRAPPA reconstruction and FLEET-ACS data (Polimeni et al., 2015) with 10° flip angle. The field of view included occipital cortical areas V1, V2, V3 and the posterior parts of V4v and V4d.

Structural (anatomical) data were acquired in a 3 T Siemens TimTrio whole-body scanner, with the standard vendor-supplied 32-channel head coil array, using a 3D T1-weighted MPRAGE sequence with protocol parameter values: TR = 2530 ms, TE= 3.39 ms, TI = 1100 ms, flip angle= 7°, BW = 200 Hz/pix, echo spacing= 8.2 ms, voxel size = 1.0 × 1.0 × 1.33 mm^3, FOV = 256 × 256 × 170 mm^3.

2.4. *General data analysis*

Functional and anatomical MRI data were pre-processed and analyzed using FreeSurfer and FS-FAST (version 6.0; http://surfer.nmr.mgh.harvard.edu/) (Fischl, 2012).

2.4.1. *Structural analysis*

For each subject, inflated and flattened cortical surfaces were reconstructed based on the high-resolution anatomical data (Dale et al., 1999; Fischl et al., 2002, 1999). During this reconstruction process, the standard pial surface was generated as the gray matter border with the surrounding cerebrospinal fluid or CSF (i.e. GM-CSF interface). The white matter surface was also generated as the interface between white and gray matter (i.e. WM-GM interface). To enable intra-cortical smoothing (see below), we also generated a family of 9 intermediated equidistant surfaces, spaced at intervals of 10 % of the cortical thickness, between WM-GM and the GM-CSF interface surfaces.

2.4.2. *Functional analysis*

All functional images were corrected for motion artifacts. For each subject, functional data from each run were rigidly aligned (6 DOF) relative to their own structural scan using rigid Boundary-Based Registration (Greve and Fischl, 2009). This procedure enabled us to compare data collected for each subject across multiple scan sessions.

To retain the spatial resolution, no tangential spatial smoothing was applied to the imaging data acquired at 7 T (i.e. 0 mm FWHM). Rather we used the more advanced method of radial (intracortical) smoothing (Blazejewska et al., 2019) – i.e. perpendicular to the cortex and within the cortical columns. The extent of this radial smoothing was limited to WM-GM interface and the adjacent 2 intermediate surfaces within the gray matter (see above) – i.e. the bottom 30 % of the gray-matter thickness starting from the WM-GM interface. This approach enabled us to increase signal- and contrast-to-noise-ratio through exploiting the prior knowledge about the columnar organization within the regions of interest (Blazejewska et al., 2019; Nasr et al., 2016; Nasr and Tootell, 2018b; Tootell and Nasr, 2021). Moreover, by not sampling from more superficial layers, we avoid spatial blurring caused by large veins at the

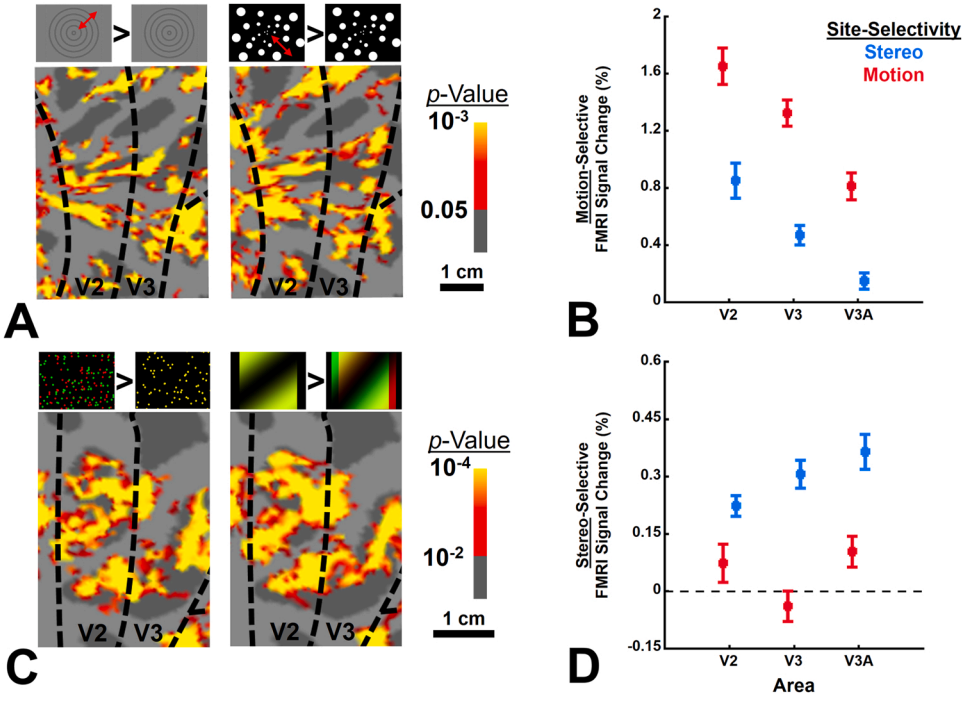

Fig. 4. The effect of changing the shape of stimuli (from gratings to random dots and vice versa) on the pattern of activity evoked within motion- and stereo-selective sites (Experiment 3). **Panels A and C** show the evoked motion and stereo-selective activity maps, respectively. For each map, the type of stimuli used in the experiment is demonstrated on top of the panel. **Panels B and D** show the level of motion- and stereo-selective activity across areas V2, V3 and V3A, evoked by random dots (Experiment 3a; $n = 11$) and gratings (Experiment 3c; $n = 11$), respectively. The regions of interest (motion- vs. stereo-selective) in each area were localized independently based on gratings and random dots. Consistent with activity maps, the level of evoked activity by 'moving vs. stationary' and '3D vs. 2D' stimuli was higher in motion- and stereo-selective sites, respectively (see also Figs. S7 and S8). These results suggest that changing the shape of stimuli does not alter the overall pattern of activity evoked within motion- and stereo-selective sites. Error bars show one standard error of mean.

pial surface (De Martino et al., 2013; Koopmans et al., 2010; Nasr et al., 2016; Polimeni et al., 2010).

A standard hemodynamic model based on a gamma function was fit to the fMRI signal to estimate the amplitude of the BOLD response. For each individual subject, the average BOLD response maps were calculated for each condition (Friston et al., 1999). Finally, voxel-wise statistical tests were conducted by computing contrasts based on a univariate general linear model, and the resultant significance maps were projected onto the subject's anatomical volumes and reconstructed cortical surfaces.

2.5. Analysis of overlap

To measure the level of overlap between sites, the selectivity maps (e.g. Fig. 1A–C) were first thresholded at $p < 0.05$. This step assured us that we were not arbitrarily assigning a label (e.g. color-selective) to a site due to noise in our measurements. Then, all thresholded values in areas V2, V3 and V3A were normalized (min-to-max were converted linearly to 0-to-1). Notably, based on our previous tests in smaller groups (Nasr et al., 2016; Tootell and Nasr, 2021), we expected comparable significance values for motion-, stereo- and color-selectivity tests (Fig. 1). Still, we used this normalization step to avoid any bias in our estimations, caused by nuisance factors such as head motion that could affect the quality of scans across sessions.

After taking these two steps, a site was called selective if the resultant normalized value for one feature (i.e. either motion, stereopsis or color) was $\sqrt{2}$ time larger than that of the value measured for any of the others. Application of this method, and the conservative (i.e. relatively low) cut-off value used in it, enabled us to expand our regions of interest by not limiting them to the centers of motion-, stereo- and color-selectivity sites. In the absence of these steps, the selectivity maps could be mostly limited to the centers of activity which reduced the size of regions of interest and increased the size of overlap between the selective sites (Figure S2).

We also measured the extent of overlap when the organization of motion-, stereo- and color-selective maps vertices was spatially 'shuffled'. For each subject, this shuffling process was repeated 10,000 times, and the averaged level of overlap was used as the chance level (for that individual). This enabled us to test whether the level of overlap between the selectivity maps was significantly above the chance level or not.

2.6. Functional connectivity analysis

Details of the functional connectivity analysis are similar to those reported previously (Nasr et al., 2016, 2015; Tootell and Nasr, 2021). Briefly, after preprocessing (see above), for each subject we removed sources of variance of non-interest including: all motion parameters measured during the motion correction procedure, the global signal, the mean signal from the portion of ventricles that were included in the acquired EPI slices, and the mean signal from a region within the deep cerebral white matter. Then, we extracted the mean BOLD signal time-course for V2/V3/V3A motion- and stereo-selective sites to use as seeds in a seed-based connectivity analysis. The correlation coefficient was computed for each of these time course seeds against the pre-processed resting-state time course data, from every voxel from the ipsilateral and contralateral hemisphere.

2.7. Time-course signal-to-noise ratio (tSNR) analysis

The time-course signal-to-noise ratio (tSNR) was defined and measured from each voxel as: mean (S) / standard deviation (S) (Triantafyllou et al., 2005), where S refers to the fMRI signal intensity during the resting-state and in the absence of any visual stimulations (eyes closed; Experiment 6).

2.8. Region of interest (ROI) analysis

ROIs including motion-, stereo- and color-selective sites across areas V2, V3 and V3A, defined for each subject based on their own data (Experiments 1 and 2) and retinotopic mapping (see above and Figure S1). To remove the impact of the fixation object presentation, only sites across 3–10° eccentricities were used in ROI analysis. This conservative approach also assured us that the evoked activity within our ROIs was not affected by the interaction (e.g. enhancement or suppression) between the stimuli and the dummy task, designed to monitor/control the subject's attention (see above).

Sites that showed overlapping selectivity were excluded from the ROIs. We did not include these sites in any analysis mainly due to their small size (Figures S3 and S4 and Tables S2-S4), which reduced the contrast-to-noise ratio of the activity that was measured within these regions. To improve sensitivity in all analyses, data from the left and right hemispheres were averaged. No hemisphere was excluded from any ROI analyses and all vertices within each ROI were used in the analyses.

2.9. Statistical data analysis

To examine the significance of independent parameters in each experiment, we used either paired t-test or repeated-measures ANOVA. Repeated-measures ANOVA is particularly susceptible to the violation of sphericity assumption, caused by the correlation between measured values and unequal variance of *differences* between experimental conditions. To address this problem, when necessary (determined using a Mauchly test), results were corrected for violation of the sphericity assumption, using the Greenhouse-Geisser method.

2.10. Data availability statement

Data and codes will be shared upon request.

3. Results

Fifteen human subjects with normal vision participated in this study (see Methods and Table S1). Each subject participated in multiple experiments, all using high-resolution fMRI (voxel size = 1 mm isotropic). Experiment 1 localized motion- and stereo-selective sites in different individuals. Experiment 2 independently confirmed that these sites are mainly under the influence of the magnocellular stream based on their none-to-minimally overlapping organization relative to color-selective sites (Experiment 2a), the higher impact of stimulus orientation on their evoked response (Experiment 2b), and their low-SF preference (Experiment 2c). Experiments 3 and 4 confirmed that the organization of these sites is largely preserved irrespective of the stimulus shape. Experiment 5 tested the selective contribution of these sites to motion direction and depth encoding. Experiment 6 tested whether sites with similar stimulus selectivity are functionally interconnected bases on an analysis of resting-state functional connectivity. Finally, Experiment 7 tested whether the level of fMRI sensitivity varied systematically between motion- and stereo-selective sites.

3.1. Experiment 1. Motion and stereopsis are encoded selectively within minimally-overlapping sites

In all participants ($n = 15$; Table S1), we first localized the cortical sites in areas V2, V3 and V3A that responded selectively to moving (compared to stationary) stimuli (Experiment 1a; Fig. 1A) and to depth-varying (compared to depth-constant) random dot stereograms (RDS; Experiment 1b; Fig. 1B). For each individual, the border of retinotopic visual areas was defined during a separate scan session (Figure S1), based on independent stimuli (Sereno et al., 1995).

As demonstrated in Fig. 1 for one individual subject, motion- (Fig. 1A) and stereo-selective (Fig. 1B) activity was often topographically elongated in a direction perpendicular to the V1-V2 border, consistent with the known topography of stripes in humans (Adams et al., 2007; Tootell and Taylor, 1995), and extended through areas V3 and V3A,. In a few subjects in which the field-of-view extended far enough (e.g. Fig. 1A), we were also able to identify the motion-selective area MT, near the posterior end of the medial temporal sulcus (Tootell et al., 1995).

When co-registered, motion- and stereo-selective sites formed two different distribution patterns (Figs. 2 and 3) with only minor spatial overlap (Figures S3 and S4 and Table S2-S4). In areas V2, V3 and V3A, this level of overlap was significantly smaller than the chance level ($t(14) > 6.95$, $p < 10^{-3}$), defined as when the selectivity maps were spatially shuffled (see Methods). Separate applications of the same test to the level of overlap between motion- and stereo-selective sites within the cortical representations of central and peripheral visual fields yielded the same results ($t(14) > 5.02$, $p < 10^{-3}$). This result provides the first direct evidence for existence of motion- and stereo-selective sites across human visual areas V2, V3 and V3A, with minimal overlap between them.

Notably, in this analysis, the size of the overlapping region was compared relative to the randomized activity maps, generated after shuffling the vertices. This procedure could reduce the level of correlation between adjacent vertices, which may increase the level of overlap between shuffled maps. Thus, our analysis does not rule out the possibility of a partial overlap between motion- and stereo-selective sites. Due to the relatively small size of the overlapping sites in areas V2 (4.53 % ± 2.58 %; normalized relative to the size V2), V3 (3.73 % ± 1.99 %) and V3A (6.54 % ± 4.33 %) (Tables S2-S4), these regions were excluded from further analysis.

3.2. Experiment 2. Motion and stereopsis are encoded within the magnocellularly-influenced sites

We tested the hypothesis that motion- and stereo-selective sites are localized within those fine-scale cortical regions that are mainly under the influence of the magnocellular stream. If true, we expected these sites: *(i)* to show no-to-minimal overlap with color-selective sites that comprise the parvocellular stream (Experiment 2a), *(ii)* to show stronger orientation selectivity compared to color-selective sites (Experiment 2b) and *(iii)* to show a preference for lower SF rather than higher SF stimuli (Experiment 2c).

3.2.1. Experiment 2a. Motion- and stereo-selective sites were localized mostly outside color-selective sites

Based on studies in NHP, we expected magnocellularly influenced sites to show no-to-minimal overlap with color-selective sites that comprise the parvocellular stream (Blasdel and Fitzpatrick, 1984; De Valois, 1965; Hubel and Livingstone, 1987; Peterhans and von der Heydt, 1993). To test this expectation, Experiment 2a localized color-selective sites based on their stronger response to isoluminant color-varying vs. luminance-varying stimuli in our participants ($n = 15$; Table S1), as in prior tests of color selectivity (Nasr et al., 2016; Nasr and Tootell, 2018a). Then the location of those color-selective stripes was compared to the location of motion- and stereo-selective sites.

Results of this test showed that, beyond area V1, color-selective sites formed a striped topography beginning at the V1-V2 border, extending through area V3 (Nasr et al., 2016) (Fig. 1C). In a few subjects for whom the field-of-view included the fusiform area (e.g. Fig. 1C), presumptive area V8/VO could also be identified in the posterior portion of middle fusiform sulcus (Hadjikhani et al., 1998; Lafer-Sousa et al., 2016; Nasr and Tootell, 2018a). However, in contrast to motion- and stereo-selective sites, color-selective sites were rarely detected within area V3A (Fig. 1C and 3 and Table S4).

Moreover, as expected from the suggested spatial segregation of magnocellular and parvocellular streams (Blasdel and Fitzpatrick, 1984; De Valois, 1965; Hubel and Livingstone, 1987; Peterhans and von der Heydt, 1993), when co-registered (Fig. 2), we found minimal overlap between motion/stereo- relative to color-selective maps (Tables S2, S3 and S4). Across areas V2 and V3, the level of this overlap was significantly below chance level ($t(14) > 4.94$, $p < 10^{-3}$), defined as when the selectivity maps were spatially shuffled. These results indicated that motion- and stereo-selective sites are preferentially located outside color-selective sites that comprise the parvocellular stream.

3.2.2. Experiment 2b. Motion- and stereo-selective sites show stronger orientation selectivity compared to color-selective sites

In NHPs, magnocellularly influenced thick stripes in V2 and their extension in other areas could be detected reliably based on their stronger orientation selectivity relative to parvocellularly influenced thin stripes (Chen et al., 2008; Kaskan et al., 2009; Lu et al., 2010; Tanigawa et al., 2010; Tootell et al., 2004; Vanduffel et al., 2002b). Accordingly, we next measured the impact of stimulus orientation on the activity evoked within motion-, stereo- and color-selective sites across areas V2 and V3. Area V3A was excluded from this test because color-selective sites were rarely detected in this area (see above).

When subjects ($n = 15$; Table S1) were presented with luminance-varying stimuli with 0°, 45°, 90° and 135° orientations (see Methods), stimulus orientation had a significantly stronger impact on the activity evoked within motion- and stereo- compared to color-selective sites across areas V2 ($t(14) = 3.56$; $p < 0.01$) and V3 ($t(14) = 2.63$; $p = 0.02$) (Figure S5). The same analysis did not yield any significant difference between the impact of stimulus orientation on the activity evoked within motion- vs. stereo-selective sites ($t(14) < 1.81$; $p > 0.10$). These results support the hypothesis that motion- and stereo-selective sites overlap the magnocellularly influenced thick stripes in V2 and their extension in V3.

It could be argued that the luminance-varying stimuli (with relatively low SF) used in this test could evoke a stronger response in those sites that were mainly under the influence of the magnocellular, rather than the parvocellular stream. This difference in stimulus preference could enhance the impacts of stimulus orientation in motion/stereo- compared to color-selective sites. To rule out this possibility, we repeated this test for the response evoked by color-varying gratings, presented to the subjects along the luminance-varying stimuli during the same scan session (see Methods). Despite the stronger activity evoked by the color-varying stimuli across color-selective sites, we did not find a significant orientation-selectivity bias in favor of color- compared to motion/stereo-selective sites in V2 ($t(14) = 1.60$, $p = 0.13$). Interestingly, in area V3, we still found a weak (but significant) orientation-selective bias in favor of motion/stereo- compared to color-selective sites ($t(14) = 1.60$, $p = 0.048$). Thus, the stronger impact of the stimulus orientation on the activity evoked within motion/stereo- compared to color-selective sites could not be solely due to their comparably stronger response to luminance-varying stimuli.

3.2.3. Experiment 2c. Motion- and stereo-selective sites show stronger preference for lower SF compared to color-selective sites

Magnocellularly influenced regions are expected to show a stronger preference for lower rather than higher SF stimulus components (Derrington and Lennie, 1984; Hicks et al., 1983). Experiment 2c compared the SF preference of motion-, stereo- and color-selective sites. When subjects ($n = 11$; Table S1) were presented with gratings with different SFs (0.1–5.79c/deg; see Methods), we found a significant SF × site-type interaction on activity evoked within areas V2 ($p < 10^{-6}$) and V3 ($p < 10^{-4}$) (see also Table S5). In both areas, motion- and stereo-selective sites showed a stronger response to gratings of lower SF (peak ≤0.27c/deg) compared to higher SF (Figure S6). In contrast, color-selective sites showed a significantly stronger response to higher SF (peak ~0.73c/deg) gratings. This result is consistent with the hypothesis that the magnocellular stream has a stronger influence on motion- and stereo-selective compared to color-selective sites. Notably, a relatively weak evoked response to higher SFs (>2c/deg) in our ROIs is consistent with the fact that these ROIs represented the peripheral visual fields (3–10°). Here again, area V3A was excluded from this test since it shows little or no color selectivity (see above).

3.3. Experiment 3. Variations in stimulus structure (shape) did not affect the organization of motion- and stereo-selective sites

In Experiment 1, we localized motion- and stereo-selective sites using gratings and RDS, respectively. The SF and orientation content of gratings (narrow band) and RDS (broad band) significantly differ from each other. To test whether the spatial organization observed in Experiment 1 were related to differences in motion and stereo, rather than differences in stimulus bandwidth, in Experiment 3 we tested whether (or not) the selectivity of activity maps changed in response to different "carrier" stimuli.

3.3.1. Experiments 3a and 3b. Use of random dots rather than gratings to activate motion-selective sites

Two independent experiments were conducted to test the effect of stimulus shape on the level of motion selectivity. In Experiments 3a, one group of subjects ($n = 11$; Table S1) was presented with random dots that, across different blocks, were either stationary or moving radially (see Methods). In Experiment 3b, another group of subjects ($n = 11$; Table S1) was presented with dots that were either stationary or moving translationally. As demonstrated in Fig. 4A and S7, the overall pattern of motion-selective activity remained similar between Experiments 1 and 3. As demonstrated in Fig. 4B, in both experiments, moving dots evoked a significantly stronger selectivity within the motion-selective sites (defined based on moving vs. stationary gratings) compared to the stereo-selective sites ($p < 10^{-3}$; see also Tables S6 and S7). These results indicate that motion-selective sites across V2, V3 and V3A areas respond selectively to motion irrespective of the carrier stimuli.

3.3.2. Experiment 3c. Use of gratings rather than RDS to activate stereo-selective sites

To test whether depth-varying stimuli other than RDS could also evoke a selective response within the stereo-selective sites, a group of subjects ($n = 11$; Table S1) were presented with depth-varying (3D) vs. depth-invariant (2D) gratings (SF=0.25c/deg) (see Methods). Here again, the pattern of stereo-selective response remained similar to that observed in Experiment 1 (Fig. 4C). As demonstrated in Fig. 4D, depth-varying stimuli evoked a significantly stronger response within the stereo-selective sites (defined based on RDS) compared to the motion-selective sites ($p < 10^{-3}$; see also Tables S8). These results indicate that stereo-selective sites across V2, V3 and V3A areas respond selectively to the stimulus binocular disparity irrespective of its spectral content. Together, the results of Experiment 3 suggest that the spatial organization of motion- and stereo-selective sites remains consistent, irrespective of the carrier stimuli (see also Experiment 4).

3.4. Experiment 4. Stereo-selective sites could be localized without disparity "oscillation"

The RDS stimuli used in Experiments 1 and 3 oscillated in depth (see Methods) to enhance 3D perception (Regan et al., 1978). This approach raised the possibility that the current spatial organization of motion- vs. stereo-selective sites reflects separated representation of two axes of motion (i.e. motion-in-depth vs. motion-in-fronto-parallel-planes). Previous studies in NHPs (Sanada and DeAngelis, 2014) and humans (Rokers et al., 2009) showed that MT activity evoked by motion-in-depth can be differentiated from activity evoked by motion-in-fronto-parallel plane. However, the contribution of earlier visual areas to this process remains unclear. Accordingly, Experiment 4 tests whether the spatial organization of motion- vs. stereo-selective sites across area V2, V3 and V3A (as shown in Experiments 1–3), represents two separate axis of motion (i.e. motion-in-depth vs. motion-in-fronto-parallel-planes).

A group of subjects ($n = 6$; Table S1) were scanned as they were presented with non-oscillating 3D vs. 2D natural scenes (Figure S8A). If the stereo-selective sites were localized based on their selectivity for motion-in-depth (rather than stereopsis per se), we expected them to lose their selectivity in this test. Alternatively, if those sites were selectively responding to the stimulus stereopsis irrespective of its oscillation, we expected the overall activity maps would remain similar

to those generated based on RDS. The results of this test showed strong stereo-selective activity evoked by non-oscillating natural scenes (Figure S8B and 8C). Importantly, the spatial distribution of stereo-selective sites across areas V2, V3 and V3A remained similar between Experiments 1 and 4 (Figure S8B) and the level of stereo-selective activity (Figure S8C) was significantly stronger within stereo-selective sites (as localized independently based on RDS) rather than motion-selective sites ($p < 0.01$; see also Tables S9). These results rule out the possibility that stereo- and motion-selective sites represent two axes of motion. Moreover, they further support the hypothesis that the spatial organization of motion- and stereo-selective sites does not depend on the stimulus spatial structure (see also Experiment 3).

3.5. Experiment 5. Selective contribution to motion direction and depth encoding

Motion-selective sites are expected to be selectively involved in discriminating stimuli based on their motion direction (An et al., 2012; Lu et al., 2010; Zimmermann et al., 2011). In Experiment 3 (see above), subjects were presented with radial (i.e. centrifugal vs. centripetal) and translational (i.e. leftward vs. rightward vs. upward vs. downward) motion (see Methods). Here, we compared the impact of motion direction on the evoked response within motion- and stereo-selective sites during those tests. For radial motion (Experiment 5a; $n = 11$; Table S1), the impact of motion direction was defined as the absolute difference between the responses evoked by centripetal vs. centrifugal motion. For translational motion (Experiment 5b; $n = 11$; Table S1), the impact of motion direction was averaged over all opponent pairs of motion directions.

In both tests (Fig. 5A and S9), we found a significantly stronger impact of motion direction on the response evoked within the motion- compared to the stereo-selective sites ($p < 0.01$; see also Tables S10 and S11). This impact weakened significantly from areas V2 to V3A ($p < 10^{-3}$), perhaps due to the simplicity of the motion stimulus used in these tests. In any event, these results support the hypothesis that, compared to stereo-selective sites, motion-selective sites contributed more strongly in signaling variation in motion direction.

By the same token, stereo-selective sites are expected to be more selectively involved in discriminating stimuli based on their stereoscopic depth (Chen et al., 2008; Nasr and Tootell, 2018b; Nienborg and Cumming, 2006; Tanabe et al., 2005). To compare the impact of depth direction on the response evoked within motion- vs. stereo-selective sites, a subset of subjects (Experiment 5c; $n = 11$; Table S1) were presented with RDS (with 0–0.2° binocular disparity), oscillating either in front (i.e. nearer to the observer) or behind the fixation fronto-parallel plane (i.e. farther) (see Methods). The impact of stimulus depth was defined as the absolute difference between the responses evoked by nearer vs. farther depths. As presented in Fig. 5B, we found a significantly stronger impact of stimulus depth on the activity evoked within stereo- compared to the motion-selective sites ($p < 0.01$; see also Table S12). Here, the overall level of this impact remained mostly the same between V2, V3, and V3A ($p = 0.63$). These results support the hypothesis that, compared to motion-selective sites, stereo-selective sites contribute more strongly in signaling depth variation.

Notably, at the first glance, a direct comparison of Fig. 5A and B may suggest that stereo-selective sites showed a higher response to motion direction rather than depth. However, Experiment 5 was not designed to answer this question. Such a comparison requires a careful adjustment of the stimulus intensities from two different modalities (i.e. motion direction vs. depth). In the absence of such adjustment, comparing the result of these two tests could be misleading.

3.6. Experiment 6. Selective functional connectivity between functionally alike versus unalike sites

We tested whether motion- and stereo-selective sites in V2, V3 and V3A, showed stronger functional connections to sites with the same ('alike') rather than different ('unalike') selectivity (Fig. 6A). If confirmed, this would support the hypothesis that motion- and stereo-selective sites comprise two channels within the magnocellular stream to process motion and stereopsis.

To test this, we used the method of resting-state functional connectivity (see Methods). Based on an independent set of scans, and in the absence of any visual input (eyes closed), we measured the level of co-fluctuations between spontaneous activity evoked within motion- and stereo-selective sites ($n = 15$; Table S1). The results (Fig. 6B) showed that, in adjacent areas, functional connections were significantly stronger between alike (i.e. motion-to-motion and stereo-to-stereo) rather than unalike sites (i.e. motion-to-stereo) ($p < 0.01$; see also Table S13). A similar result was found when we tested the functional connection between contralateral hemispheres (Fig. 6C). The latter result ruled out the possibility that the selective functional connectivity between alike sites could be due to the smaller distance between them, compared to unalike sites. Together, these results supported the hypothesis that motion- and stereo-selective sites comprise two fine-scale channels within the magnocellular stream. Notably, this result could not be attributed to a common sensory input, because all recordings were conducted during the resting-state with eyes closed.

3.7. Experiment 7. Equivalent fMRI sensitivity in motion- vs. stereo-selective sites

It could be argued that at least parts of the findings in Experiments 1–6 were due to the differences in fMRI sensitivity between motion- and stereo-selective sites. To test this hypothesis directly, we compared the tSNR of the fMRI signal (Triantafyllou et al., 2005), collected within

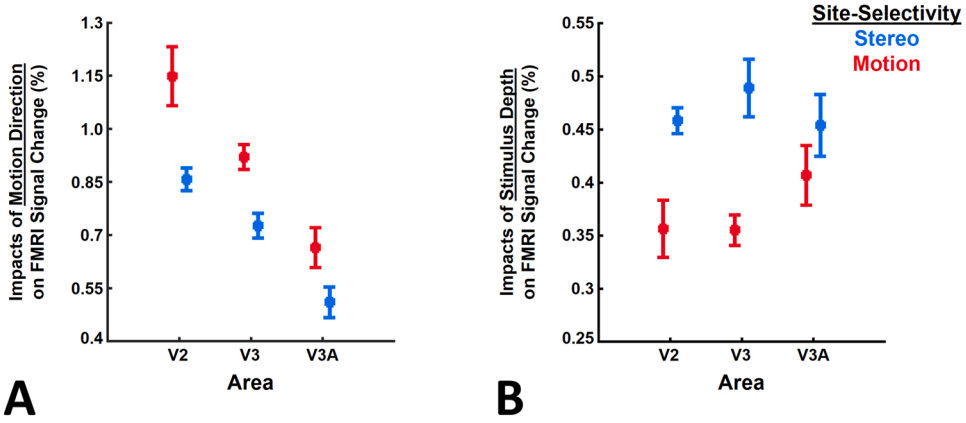

Fig. 5. The impact of the stimulus motion direction and depth on the evoked response measured across motion- and stereo-selective sites (Experiment 5). **Panel A** shows the impact of motion direction (centrifugal vs. centripetal) across different ROIs ($n = 11$). **Panel B** shows the impact of stimulus depth (in front vs. behind the fixation target) ($n = 11$). The impact of motion direction and depth was stronger on the activity evoked within motion- and stereo-selective sites, respectively. Error bars show one standard error of mean.

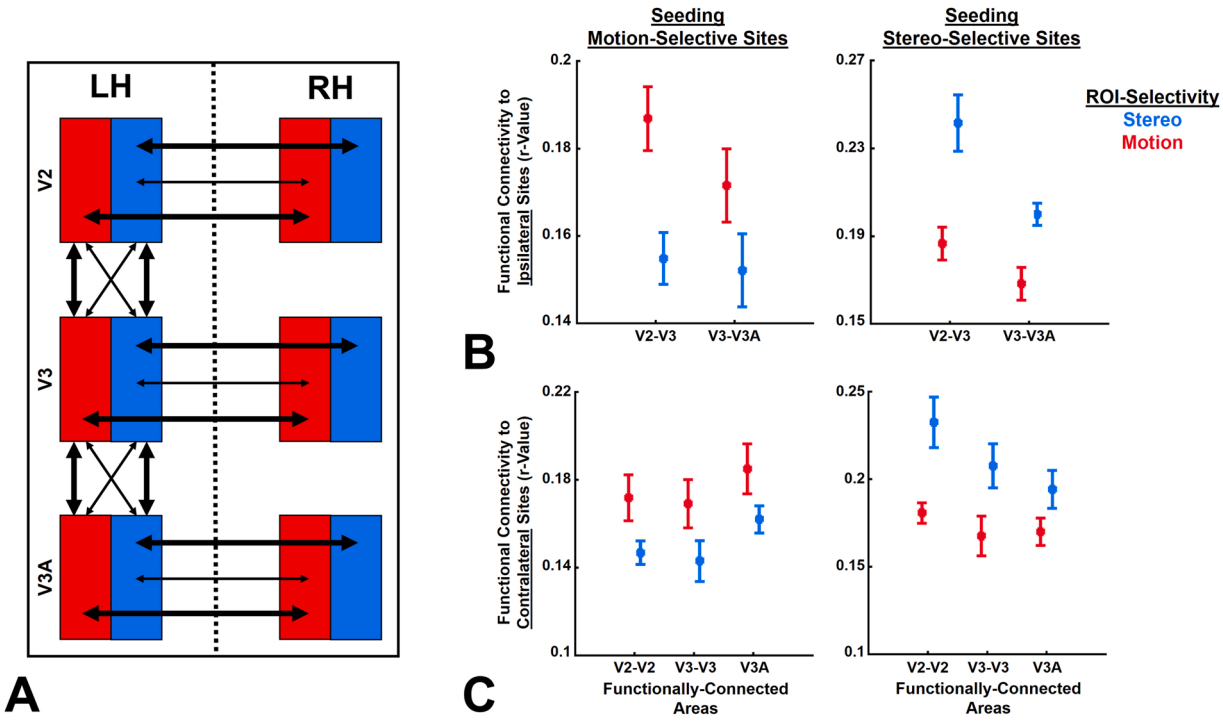

Fig. 6. – The functional connection between ipsilateral and contralateral ROIs measured during resting-state with closed eyes (Experiment 6; $n = 15$). **Panel A** shows a schematic representation of the proposed hypothesis about the functional connection between the sites. Motion- and stereo-selective sites are depicted as red and blue boxes, respectively. Stronger/weaker functional connections are also depicted with thick/thin arrows. **Panel B** shows the level of functional connectivity between V2-V3 and V3-V3A. Here, the seeded areas and the ROIs were located within the same hemisphere. **Panel C** shows the level of functional connectivity between the two hemispheres (i.e. the seeded area and the ROI were located contralaterally). In **Panels B and C**, the left vs. right column show the results of seeding motion vs. stereo-selective sites. In each hemisphere, motion- and stereo-selective sites show stronger functional connectivity to ipsilateral and contralateral sites with the same (alike) rather than different (unalike) selectivity. Error bars show one standard error of mean.

motion- and stereo-selective sites across V2, V3, and V3A during the resting-state and in the absence of any visual stimulation ($n = 15$; Table S1). Results of this test (Figure S10) did not yield any significant differences between tSNR measured within motion- vs. stereo-selective sites, across areas V2 ($t(14) = 1.37$, $p = 0.19$), V3 ($t(14) = 1.31$, $p = 0.21$) and V3A ($t(14) = 0.99$, $p = 0.34$). This result ruled out the possibility that fMRI sensitivity differed systematically between motion- and stereo-selective sites.

4. Discussion

For decades, the concept of segregated magnocellular vs. parvocellular pathways shaped our understanding of distributed neuronal processing across visual areas (Felleman and Van Essen, 1991; Hubel and Livingstone, 1987; Tootell and Nasr, 2017; Zeki and Shipp, 1988). Here we provide direct evidence for the existence of two minimally-overlapping mesoscale processing channels within the magnocellular stream that selectively contribute to motion and stereopsis encoding. As we discuss below, the existence of such fine-scale channels in human extrastriate visual cortex was completely unknown to us and could not be predicted based on animal models. This is an important milestone for studying human brain function, especially in those regions that are likely different between humans and NHPs (e.g. V3 and V3A).

4.1. Consistent but beyond animal models for area V2

According to previous studies in NHPs, V2 motion- (An et al., 2012; Hu et al., 2018; Lu et al., 2010) and stereo-selective sites (Chen et al., 2008; Li et al., 2017; Roe and Ts'o, 1995) were localized mainly within thick stripes. These sites that comprise the magnocellular stream also showed strong orientation selectivity (Kaskan et al., 2009; Vanduffel et al., 2002b) and weak-to-no color-selective response (Lu and Roe, 2008; Tootell et al., 2004). However, none of these studies tested for the relative organization of motion- vs. stereo-selective sites.

Consistent with these studies in NHPs, Experiment 2 showed that motion/stereo-selective sites in human V2 showed little overlap with color-selective sites. We also found a stronger orientation-selective response in motion/stereo- compared to color-selective sites. Moreover, we showed evidence for differential SF preference in motion/stereo- vs. color-selective sites as expected from the differential influence of magnocellular vs. parvocellular streams on these sites (Derrington and Lennie, 1984; Hicks et al., 1983). Thus, our findings regarding the overall organization of motion/stereo- vs. color-selective sites, plus a stronger influence of the magnocellular stream on the function of motion/stereo-selective sites are consistent with previous reports in NHPs.

However, the evidence provided here for the minimally overlapping organization of motion- and stereo-selective sites within area V2 could not be predicted from previous studies in NHPs. This is mainly because, methodological limitations (e.g. time constrains for conducting multiple tests) prohibited those studies from localizing motion- and stereo-selective sites within the same animal. This said, our current findings do not rule out the possibility that a homologous organization may also exist in NHPs. But, in the absence of such evidence the relative organization of these sites in NHP remains unclear.

4.2. Limited knowledge of area V3 in NHPs

Our knowledge of area V3 in NHPs is relatively limited. Although many studies have reported color-, motion-, stereo- and orientation-selective sites within this area (Anzai et al., 2011; Felleman and Van Essen, 1987; Gegenfurtner et al., 1997; Tootell et al., 2004; Tsao et al., 2003; Vanduffel et al., 2002b), the relative organization of these sites is still a matter of debate. For instance, while Tanigawa and colleagues

suggested a segregated organization of color- and orientation-selective sites within areas V3 (Tanigawa et al., 2010), earlier studies reported a significant overlap between these sites (Felleman and Van Essen, 1987; Gegenfurtner et al., 1997). Considering this, plus the smaller size of V3 in NHPs compared to humans (Orban et al., 2004; Sereno and Tootell, 2005), it would have been challenging to predict our current findings from the animal model.

4.3. V3A in humans vs. NHPs

Our knowledge of homology between area V3A in humans vs. NHPs is also relatively limited. On the one hand, multiple studies have reported stereo-selective activity in area V3A of humans (Goncalves et al., 2015; Nasr et al., 2016; Nasr and Tootell, 2018b; Neri et al., 2004; Ng et al., 2021; Tsao et al., 2003) and NHPs (Anzai et al., 2011; Tsao et al., 2003; Vanduffel et al., 2002a). In both species, color-selective sites are rarely found in this region (Hadjikhani et al., 1998; Tootell and Nasr, 2017; Tootell et al., 2004).

On the other hand, V3A contribution to motion encoding may differ between humans and NHPs. Specifically, a group of neuroimaging studies have suggested that motion-selective activity in V3A is limited to humans (Orban et al., 2003; Vanduffel et al., 2001). While others, based on using single-cell recording, have shown evidence for motion-selective neurons in this area (Galletti et al., 1990; Nakhla et al., 2021; Zeki, 1978). Thus, our reported non-overlapping organization of motion- and stereo-selective sites in area V3A may (or may not) be limited to humans.

4.4. The level of overlap between motion- and stereo-selective sites

Ideally, the overlap between motion- and stereo-selective sites should be localized independently based on the functional characteristics of this region. For instance, this region may show a selective response to the perceptual interaction between the stimulus motion and depth as in motion parallax (Gibson et al., 1959). However, considering our limited knowledge of these overlapping regions, the introduction of such functional localizers requires more assessments in future. Moreover, considering the small size of these overlapping regions, such a measurement requires ultra-high spatial resolution beyond what is currently available to us (also see Section 4.7).

In the absence of an independent localizer for detecting the overlapping regions, it could be argued that, by using a relatively small cut-off value (see Methods), we have underestimated the level of overlap between motion- and stereo-selective sites (see also Figure S2). However, the results of Experiments 5 and 6 suggest that our approach did not prohibit us from differentiating the function of motion- and stereo-selective sites. Specifically, Experiment 5 differentiated the impacts of motion direction and depth on the evoked response within motion- and stereo-selective sites. Experiment 6 also revealed a selective functional connectivity between ipsilateral and contralateral sites with alike stimulus selectivity. Thus, the potential errors in detection of the overlapping sites appear to be small.

4.5. Selective but not necessarily segregated functional connectivity between alike sites

Previously we showed evidence for selective functional connectivity between “stereo- vs. color-selective” (Nasr et al., 2016) and “motion- vs. color-selective” (Tootell and Nasr, 2021) sites. Here, we extend those findings by showing that such a selective functional connection also exists between “motion- vs. stereo-selective” sites. This finding supports the existence of two fine-scale channels within the magnocellular stream.

However, the nature of interaction between these two channels remains unknown. Notably, in our resting-state analysis, the level of correlation between unalike sites remained significantly above zero. Thus, these two channels may still show some levels of interaction. Existence of such an interaction is consistent with the behavioral findings that stimulus motion may influence depth processing (Regan et al., 1978) and that motion parallax may be used as an independent cue in depth perception (Gibson et al., 1959). The specific nature of this interaction needs to be assessed in the future (also see (Sincich and Horton, 2005)).

4.6. Heterogeneity and between-subjects-variability in representation of motion- vs. stereo-selective sites across individuals

Our findings (Figs. 2 and 3) suggest a heterogeneity in spatial distribution of motion- and stereo-selective sites across visual areas V2, V3, and V3A. Generally, the existence of such a heterogeneity, especially in fine-scales, is not a surprise. For instance, in NHPs (Tootell et al., 1983) and humans (Nasr et al., 2016), compared to motion- and stereo-selective sites, color-selective sites are more frequently found near the V1/V2 border. In both species, near- and far-preferring stereo-selective sites are also distributed heterogeneously within dorsal and ventral portions of the visual area (Adams and Zeki, 2001; Chen et al., 2008; Nasr and Tootell, 2018b). However, the underlying cause of these heterogeneities is still mostly unknown.

One exciting possibility is the biases in statistics of natural scenes and their impacts on the development of the visual system (Yang and Purves, 2003). If true, one may expect (at least) some similarities in the distribution of stereo- and motion-selective sites across different individuals. At first glance, such a similarity is not apparent in our current results (Fig. 2B and 3B). However, we cannot rule out the possibility that advanced image processing methods may still reveal such a similarity, and clarify the link between those patterns and the behavioral bias in visual perception (see also (Nasr and Tootell, 2020)). Notably, the between-subjects-variability in distribution and size of motion- and stereo-selective sites may be (at least partly) due to the difference in perceptual capabilities across subjects, beyond what was measured by our behavioral tests (see Methods).

4.7. Limitations

Despite the recent improvements in fMRI, the limited spatial resolution of this technique still prohibits us from assessing the fine-scale organization of many brain regions. For instance, although the current study focused on extrastriate cortex, similar questions could also be explored in the striate visual cortex (V1) and the lateral geniculate nucleus (LGN) of the thalamus. In both regions, magnocellular and parvocellular streams are expected to influence separate sites (Derrington et al., 1984; Derrington and Lennie, 1984; Hicks et al., 1983; Livingstone and Hubel, 1982; Tootell et al., 1988a, 1988b). However, the spatial resolution used here (1 mm isotropic) was inadequate to differentiate these sites.

The same limitation biased our findings toward larger motion-, stereo-, and color-selective sites and likely prohibited us from detecting smaller (sub-millimeter) sites. Such a bias may contribute to the apparent heterogeneity in distribution of these sites across visual areas as discussed before (see also Figs. 2 and 3). It also prohibited us from examining the function of the small overlapping regions due to the low contrast-to-noise ratio in these small regions.

The other technical difficulty, that affected our capabilities to assess more brain regions, was the limited scan coverage. For the majority of our subjects, our scan coverage did not include the anterior portion of area V4. For those in whom we had access to area V4 (Figs. 1–3A), we noticed the same functional organization (i.e. minimally overlapping color-, motion- and stereo-selective sites) as we detected in the earlier areas. Also, in those individuals for whom we had access to the posterior tip of medial temporal sulcus, we could localize area MT based on its selectivity for motion and the absence of selectivity for color (Tootell et al., 1995; Tootell and Taylor, 1995). Unfortunately, the small number of these cases kept us from expanding our conclusion to those areas.

Notably, in almost all fMRI studies, the expansion of sampling area requires either a decrease in the spatial resolution or a decrease in signal-to-noise ratio. To achieve these goals simultaneously, a combination of stronger MR scanners (Triantafyllou et al., 2005), more advanced data acquisition sequences (e.g. (Berman et al., 2020)) and more efficient data processing methods (e.g. (Polimeni et al., 2017; Wang et al., 2022)) will be required in the future.

5. Conclusion

Until recently, applications of fMRI have been mostly limited to localization of large-scale brain areas and assessing their function across various experimental conditions. This has changed with introduction of high-resolution fMRI using ultra-high field scanners (e.g. 7 or 9.4 Tesla). Using advanced technologies and the state-of-the-art scanners, many groups have revealed mesoscale structures within the spatial scale of cortical columns in human striate (Cheng et al., 2001; Nasr et al., 2016; Yacoub et al., 2007) and extrastriate cortex (Nasr et al., 2016; Ng et al., 2021; Tootell and Nasr, 2021; Zimmermann et al., 2011). For understandable reasons, these studies typically limited themselves to replicating what was already known to us based on animal models. However, with improvement in the reliability of fMRI, the present study demonstrates how human fMRI studies can be used to test new hypotheses beyond what was already known to us based on animal models.

Data Availability

Data will be made available on request.

Acknowledgment

This work was supported by NIH NEI (grants R01EY026881 and R01EY030434), and by the MGH/HST Athinoula A. Martinos Center for Biomedical Imaging. Crucial resources were made available by a NIH Shared Instrumentation Grant S10-RR019371. We thank Ms. Azma Mareyam for help with hardware maintenance during this study and Dr. Anna Blazejewska for her helps with implementing the method of radial smoothing. We also thank Drs. Roger Tootell, Bruce Rosen, Anna Roe, Haidong Lu, Ichiro Fujita, Gregory DeAngelis and Akiyuki Anzai for their helpful comments.

Appendix A. Supporting information

Supplementary data associated with this article can be found in the online version at doi:10.1016/j.pneurobio.2022.102374.

References

Adams, D.L., Zeki, S., 2001. Functional organization of macaque V3 for stereoscopic depth. J. Neurophysiol. 86, 2195–2203.
Adams, D.L., Sincich, L.C., Horton, J.C., 2007. Complete pattern of ocular dominance columns in human primary visual cortex. J. Neurosci. 27, 10391–10403.
Adams, W.J., Elder, J.H., Graf, E.W., Leyland, J., Lugtigheid, A.J., Muryy, A., 2016. The southampton-york natural scenes (syns) dataset: statistics of surface attitude. Sci. Rep. 6, 1–17.
Albright, T.D., Desimone, R., Gross, C.G., 1984. Columnar organization of directionally selective cells in visual area MT of the macaque. J. Neurophysiol. 51, 16–31.
An, X., Gong, H., Qian, L., Wang, X., Pan, Y., Zhang, X., Yang, Y., Wang, W., 2012. Distinct functional organizations for processing different motion signals in V1, V2, and V4 of macaque. J. Neurosci. 32, 13363–13379.
Anzai, A., Chowdhury, S.A., DeAngelis, G.C., 2011. Coding of stereoscopic depth information in visual areas V3 and V3A. J. Neurosci. 31, 10270–10282.
Berman, A.J., Grissom, W.A., Witzel, T., Nasr, S., Park, D.J., Setsompop, K., Polimeni, J. R., 2020. Ultra-high spatial resolution BOLD fMRI in humans using combined segmented-accelerated VFA-FLEET with a recursive RF pulse design. Magn. Reson. Med. 85, 120–139.
Blasdel, G.G., Fitzpatrick, D., 1984. Physiological organization of layer 4 in macaque striate cortex. J. Neurosci. 4, 880–895.
Blazejewska, A.I., Fischl, B., Wald, L.L., Polimeni, J.R., 2019. Intracortical smoothing of small-voxel fMRI data can provide increased detection power without spatial resolution losses compared to conventional large-voxel fMRI data. Neuroimage 189, 601–614.
Bone, R.A., Landrum, J.T., 2004. Heterochromatic flicker photometry. Arch. Biochem. Biophys. 430, 137–142.
Brainard, D.H., 1997. The psychophysics toolbox. Spat. Vis. 10, 433–436.
Chen, G., Lu, H.D., Roe, A.W., 2008. A map for horizontal disparity in monkey V2. Neuron 58, 442–450.
Cheng, K., Waggoner, R.A., Tanaka, K., 2001. Human ocular dominance columns as revealed by high-field functional magnetic resonance imaging. Neuron 32, 359–374.
Dale, A.M., Fischl, B., Sereno, M.I., 1999. Cortical surface-based analysis. I. Segmentation and surface reconstruction. Neuroimage 9, 179–194.
De Martino, F., Zimmermann, J., Muckli, L., Ugurbil, K., Yacoub, E., Goebel, R., 2013. Cortical depth dependent functional responses in humans at 7T: improved specificity with 3D GRASE. PLoS One 8, e60514.
De Valois, R.L, 1965. Analysis and coding of color vision in the primate visual system. Cold Spring Harb. Symp. Quant. Biol. Cold Spring Harbor Laboratory Press, p. 567.
DeAngelis, G.C., Newsome, W.T., 1999. Organization of disparity-selective neurons in macaque area MT. J. Neurosci. 19, 1398–1415.
DeAngelis, G.C., Newsome, W.T., 2004. Perceptual "read-out" of conjoined direction and disparity maps in extrastriate area MT. PLoS Biol. 2, E77.
DeAngelis, G.C., Uka, T., 2003. Coding of horizontal disparity and velocity by MT neurons in the alert macaque. J. Neurophysiol. 89, 1094–1111.
Derrington, A.M., Lennie, P., 1984. Spatial and temporal contrast sensitivities of neurones in lateral geniculate nucleus of macaque. J. Physiol. 357, 219–240.
Derrington, A.M., Krauskopf, J., Lennie, P., 1984. Chromatic mechanisms in lateral geniculate nucleus of macaque. J. Physiol. 357, 241–265.
Felleman, D.J., Essen, D.C, Van, 1987. Receptive field properties of neurons in area V3 of macaque monkey extrastriate cortex. J. Neurophysiol. 57, 889–920.
Felleman, D.J., Essen, D.C, Van, 1991. Distributed hierarchical processing in the primate cerebral cortex. Cereb. Cortex 1, 1–47.
Fischl, B., 2012. FreeSurfer. Neuroimage 62, 774–781.
Fischl, B., Sereno, M.I., Dale, A.M., 1999. Cortical surface-based analysis. II: Inflation, flattening, and a surface-based coordinate system. NeuroImage 9, 195–207.
Fischl, B., Salat, D.H., Busa, E., Albert, M., Dieterich, M., Haselgrove, C., van der Kouwe, A., Killiany, R., Kennedy, D., Klaveness, S., Montillo, A., Makris, N., Rosen, B., Dale, A.M., 2002. Whole brain segmentation: automated labeling of neuroanatomical structures in the human brain. Neuron 33, 341–355.
Friston, K.J., Holmes, A.P., Price, C.J., Buchel, C., Worsley, K.J., 1999. Multisubject fMRI studies and conjunction analyses. Neuroimage 10, 385–396.
Galletti, C., Battaglini, P.P., Fattori, P., 1990. 'Real-motion' cells in area V3A of macaque visual cortex. Exp. Brain Res. 82, 67–76.
Gegenfurtner, K.R., Kiper, D.C., Levitt, J.B., 1997. Functional properties of neurons in macaque area V3. J. Neurophysiol. 77, 1906–1923.
Gibson, E.J., Gibson, J.J., Smith, O.W., Flock, H., 1959. Motion parallax as a determinant of perceived depth. J. Exp. Psychol. 58, 40.
Goncalves, N.R., Ban, H., Sanchez-Panchuelo, R.M., Francis, S.T., Schluppeck, D., Welchman, A.E., 2015. 7 tesla FMRI reveals systematic functional organization for binocular disparity in dorsal visual cortex. J. Neurosci. 35, 3056–3072.
Greve, D.N., Fischl, B., 2009. Accurate and robust brain image alignment using boundary-based registration. NeuroImage 48, 63–72.
Hadjikhani, N., Liu, A.K., Dale, A.M., Cavanagh, P., Tootell, R.B., 1998. Retinotopy and color sensitivity in human visual cortical area V8. Nat. Neurosci. 1, 235–241.
Hicks, T.P., Lee, B.B., Vidyasagar, T.R., 1983. The responses of cells in macaque lateral geniculate nucleus to sinusoidal gratings. J. Physiol. 337, 183–200.
Hu, J., Ma, H., Zhu, S., Li, P., Xu, H., Fang, Y., Chen, M., Han, C., Fang, C., Cai, X., 2018. Visual motion processing in macaque V2. Cell Rep. 25 (e155), 157–167.
Hubel, D.H., Livingstone, M.S., 1987. Segregation of form, color, and stereopsis in primate area 18. J. Neurosci. 7, 3378–3415.
Ives, F.E., 1907. A new color meter. J. Frankl. Inst. 164, 47–56.
Kaskan, P.M., Lu, H.D., Dillenburger, B.C., Kaas, J.H., Roe, A.W., 2009. The organization of orientation-selective, luminance-change and binocular- preference domains in the second (V2) and third (V3) visual areas of New World owl monkeys as revealed by intrinsic signal optical imaging. Cereb. Cortex 19, 1394–1407.
Koopmans, P.J., Barth, M., Norris, D.G., 2010. Layer-specific BOLD activation in human V1. Hum. Brain Mapp. 31, 1297–1304.
Krug, K., Parker, A.J., 2011. Neurons in dorsal visual area V5/MT signal relative disparity. J. Neurosci. 31, 17892–17904.
Lafer-Sousa, R., Conway, B.R., Kanwisher, N.G., 2016. Color-biased regions of the ventral visual pathway lie between face-and place-selective regions in humans, as in macaques. J. Neurosci. 36, 1682–1697.
Li, X., Zhu, Q., Janssens, T., Arsenault, J.T., Vanduffel, W., 2017. In vivo identification of thick, thin, and pale stripes of macaque area V2 using submillimeter resolution (f) MRI at 3 T. Cereb. Cortex 29, 544–560.
Livingstone, M.S., Hubel, D.H., 1982. Thalamic inputs to cytochrome oxidase-rich regions in monkey visual cortex. Proc. Natl. Acad. Sci. USA 79, 6098–6101.
Lu, H.D., Roe, A.W., 2008. Functional organization of color domains in V1 and V2 of macaque monkey revealed by optical imaging. Cereb. Cortex 18, 516–533.
Lu, H.D., Chen, G., Tanigawa, H., Roe, A.W., 2010. A motion direction map in macaque V2. Neuron 68, 1002–1013.
Maunsell, J.H., Essen, D.C, Van, 1983. Functional properties of neurons in middle temporal visual area of the macaque monkey. II. Binocular interactions and sensitivity to binocular disparity. J. Neurophysiol. 49, 1148–1167.
Maunsell, J.H., Nealey, T.A., DePriest, D.D., 1990. Magnocellular and parvocellular contributions to responses in the middle temporal visual area (MT) of the macaque monkey. J. Neurosci. 10, 3323–3334.

Nakhla, N., Korkian, Y., Krause, M.R., Pack, C.C., 2021. Neural selectivity for visual motion in macaque area V3A. Eneuro 8.
Nasr, S., Tootell, R.B., 2018a. Columnar organization of mid-spectral and end-spectral hue preferences in human visual cortex. Neuroimage.
Nasr, S., Tootell, R.B., 2018b. Visual field biases for near and far stimuli in disparity selective columns in human visual cortex. Neuroimage 168, 358–365.
Nasr, S., Tootell, R.B., 2020. Asymmetries in global perception are represented in near- versus far-preferring clusters in human visual cortex. J. Neurosci. 40, 355–368.
Nasr, S., Stemmann, H., Vanduffel, W., Tootell, R.B., 2015. Increased visual stimulation systematically decreases activity in lateral intermediate cortex. Cereb. Cortex 25, 4009–4028.
Nasr, S., Polimeni, J.R., Tootell, R.B., 2016. Interdigitated color- and disparity-selective columns within human visual cortical areas V2 and V3. J. Neurosci. 36, 1841–1857.
Neri, P., Bridge, H., Heeger, D.J., 2004. Stereoscopic processing of absolute and relative disparity in human visual cortex. J. Neurophysiol. 92, 1880–1891.
Ng, A.K., Jia, K., Goncalves, N.R., Zamboni, E., Kemper, V.G., Goebel, R., Welchman, A. E., Kourtzi, Z., 2021. Ultra-high-field neuroimaging reveals fine-scale processing for 3D perception. J. Neurosci. 41, 8362–8374.
Nienborg, H., Cumming, B.G., 2006. Macaque V2 neurons, but not V1 neurons, show choice-related activity. J. Neurosci. 26, 9567–9578.
Orban, G.A., Fize, D., Peuskens, H., Denys, K., Nelissen, K., Sunaert, S., Todd, J., Vanduffel, W., 2003. Similarities and differences in motion processing between the human and macaque brain: evidence from fMRI. Neuropsychologia 41, 1757–1768.
Orban, G.A., Van Essen, D., Vanduffel, W., 2004. Comparative mapping of higher visual areas in monkeys and humans. Trends Cogn. Sci. 8, 315–324.
Pelli, D.G., 1997. The VideoToolbox software for visual psychophysics: transforming numbers into movies. Spat. Vis. 10, 437–442.
Peterhans, E., von der Heydt, R., 1993. Functional organization of area V2 in the alert macaque. Eur. J. Neurosci. 5, 509–524.
Polimeni, J.R., Fischl, B., Greve, D.N., Wald, L.L., 2010. Laminar analysis of 7T BOLD using an imposed spatial activation pattern in human V1. Neuroimage 52, 1334–1346.
Polimeni, J.R., Bhat, H., Witzel, T., Benner, T., Feiweier, T., Inati, S.J., Renvall, V., Heberlein, K., Wald, L.L., 2015. Reducing sensitivity losses due to respiration and motion in accelerated echo planar imaging by reordering the autocalibration data acquisition. Magn. Reson. Med.
Polimeni, J.R., Renvall, V., Zaretskaya, N., Fischl, B., 2017. Analysis strategies for high-resolution UHF-fMRI data. Neuroimage.
Regan, D., Beverley, K., Cynader, M., 1978. Stereoscopic depth channels for position and for motion. Frontiers in Visual Science. Springer, pp. 351–372.
Roe, A.W., Ts'o, D.Y., 1995. Visual topography in primate V2: multiple representation across functional stripes. J. Neurosci. 15, 3689–3715.
Rokers, B., Cormack, L.K., Huk, A.C., 2009. Disparity-and velocity-based signals for three-dimensional motion perception in human MT+. Nat. Neurosci. 12, 1050.
Sanada, T.M., DeAngelis, G.C., 2014. Neural representation of motion-in-depth in area MT. J. Neurosci. 34, 15508–15521.
Sereno, M.I., Tootell, R.B., 2005. From monkeys to humans: what do we now know about brain homologies? Curr. Opin. Neurobiol. 15, 135–144.
Sereno, M.I., Dale, A.M., Reppas, J.B., Kwong, K.K., Belliveau, J.W., Brady, T.J., Rosen, B.R., Tootell, R.B., 1995. Borders of multiple visual areas in humans revealed by functional magnetic resonance imaging. Science 268, 889–893.
Shipp, S., Zeki, S., 2002. The functional organization of area V2, I: specialization across stripes and layers. Vis. Neurosci. 19, 187–210.
Sincich, L.C., Horton, J.C., 2005. The circuitry of V1 and V2: integration of color, form, and motion. Annu. Rev. Neurosci. 28, 303–326.
Tanabe, S., Doi, T., Umeda, K., Fujita, I., 2005. Disparity-tuning characteristics of neuronal responses to dynamic random-dot stereograms in macaque visual area V4. J. Neurophysiol. 94 (2683–2699).
Tanigawa, H., Lu, H.D., Roe, A.W., 2010. Functional organization for color and orientation in macaque V4. Nat. Neurosci. 13 (1542).
Thomas, O.M., Cumming, B.G., Parker, A.J., 2002. A specialization for relative disparity in V2. Nat. Neurosci. 5, 472–478.
Tootell, R.B., Nasr, S., 2017. Columnar segregation of magnocellular and parvocellular streams in human extrastriate cortex. J. Neurosci. 37, 8014–8032.
Tootell, R.B., Nasr, S., 2021. Scotopic vision is selectively processed in thick-type columns in human extrastriate cortex. Cereb. Cortex 31, 1163–1181.
Tootell, R.B., Taylor, J.B., 1995. Anatomical evidence for MT and additional cortical visual areas in humans. Cereb. Cortex 5, 39–55.
Tootell, R.B., Silverman, M.S., De Valois, R.L., Jacobs, G.H., 1983. Functional organization of the second cortical visual area in primates. Science 220, 737–739.
Tootell, R.B., Hamilton, S.L., Switkes, E., 1988a. Functional anatomy of macaque striate cortex. IV. Contrast and magno-parvo streams. J. Neurosci. 8, 1594–1609.
Tootell, R.B., Silverman, M.S., Hamilton, S.L., De Valois, R.L., Switkes, E., 1988b. Functional anatomy of macaque striate cortex. III. Color. J. Neurosci. 8, 1569–1593.
Tootell, R.B., Reppas, J.B., Kwong, K.K., Malach, R., Born, R.T., Brady, T.J., Rosen, B.R., Belliveau, J.W., 1995. Functional analysis of human MT and related visual cortical areas using magnetic resonance imaging. J. Neurosci. 15, 3215–3230.
Tootell, R.B., Nelissen, K., Vanduffel, W., Orban, G.A., 2004. Search for color 'center(s)' in macaque visual cortex. Cereb. Cortex 14, 353–363.
Triantafyllou, C., Hoge, R.D., Krueger, G., Wiggins, C.J., Potthast, A., Wiggins, G.C., Wald, L.L., 2005. Comparison of physiological noise at 1.5 T, 3 T and 7 T and optimization of fMRI acquisition parameters. Neuroimage 26, 243–250.
Tsao, D.Y., Vanduffel, W., Sasaki, Y., Fize, D., Knutsen, T.A., Mandeville, J.B., Wald, L.L., Dale, A.M., Rosen, B.R., Van Essen, D.C., Livingstone, M.S., Orban, G.A., Tootell, R. B., 2003. Stereopsis activates V3A and caudal intraparietal areas in macaques and humans. Neuron 39, 555–568.
Vanduffel, W., Fize, D., Mandeville, J.B., Nelissen, K., Van Hecke, P., Rosen, B.R., Tootell, R.B., Orban, G.A., 2001. Visual motion processing investigated using contrast agent-enhanced fMRI in awake behaving monkeys. Neuron 32, 565–577.
Vanduffel, W., Fize, D., Peuskens, H., Denys, K., Sunaert, S., Todd, J., Orban, G., 2002a. Extracting 3D from motion: differences in human and monkey intraparietal cortex. Science 298, 413–415.
Vanduffel, W., Tootell, R.B., Schoups, A.A., Orban, G.A., 2002b. The organization of orientation selectivity throughout macaque visual cortex. Cereb. Cortex 12, 647–662.
Wang, J., Nasr, S., Roe, A.W., Polimeni, J.R. (2022) Critical factors in achieving fine-scale functional MRI: Removing sources of inadvertent spatial smoothing. Wiley Online Library.
Yacoub, E., Shmuel, A., Logothetis, N., Ugurbil, K., 2007. Robust detection of ocular dominance columns in humans using Hahn Spin Echo BOLD functional MRI at 7 Tesla. Neuroimage 37, 1161–1177.
Yang, Z., Purves, D., 2003. A statistical explanation of visual space. Nat. Neurosci. 6, 632–640.
Zeki, S., 1978. The third visual complex of rhesus monkey prestriate cortex. J. Physiol. 277, 245–272.
Zeki, S., Shipp, S., 1988. The functional logic of cortical connections. Nature 335, 311–317.
Zimmermann, J., Goebel, R., De Martino, F., van de Moortele, P.F., Feinberg, D., Adriany, G., Chaimow, D., Shmuel, A., Ugurbil, K., Yacoub, E., 2011. Mapping the organization of axis of motion selective features in human area MT using high-field fMRI. PLoS One 6, e28716.